Supplementary Information (SI)

Ultra-confined plasmons reveal moiré patterns in twisted bilayer graphene–talc heterostructure

Tiago C. Barbosa [1,2], Andre J. Chaves [3], Raul O. Freitas [4], Leonardo C. Campos [1,2], and Ingrid D. Barcelos [4]

[1]Departamento de Física, Universidade Federal de Minas Gerais (UFMG), Belo Horizonte, MG, 31270-901, Brasil.

[2]Centro de Tecnologia em Nanomateriais e Grafeno, Universidade Federal de Minas Gerais, Belo Horizonte, MG, 31270-901, Brasil.

[3]Department of Physics, Aeronautics Institute of Technology, 12228-900, São José dos Campos, SP, Brazil

[4]Laboratório Nacional de Luz Síncrotron (LNLS), Centro Nacional de Pesquisa em Energia e Materiais (CNPEM), Campinas, SP, 13083-970, Brasil.

January 31, 2025

1 The twisted bilayer graphene reconstruction regime

When two graphene layers are stacked to form a twisted bilayer graphene (TBG), their lattices create a new periodic array, called moiré pattern (Fig. S1a), introducing twist-angle-dependent features in the electronic, optical, and mechanical properties [1]. At twist angles below the so called "magic angle", i. e., 1.1^{o}, the system undergoes a self-organized lattice reconstruction which we describe further in this section. In this regime, the structure of the TBG is governed by the interplay between interlayer van der Waals interaction, which arises from stacking two layers, and the in-plane strain field, which arises from the atomic mismatch between these layers [2]. As a result, the interaction between the graphene layers lead to atomic relaxations that minimize the total energy by increasing the Bernal (AB and BA) stacking areas

while decreasing the AA-stacking regions [3]. Therefore, the resulting reconstructed lattice is composed of periodic triangular areas of alternating Bernal stacking domains, separated by shear soliton regions, with AA-stacked regions at the vertices of the triangles (Fig. S1b), which is the minimum energy state.

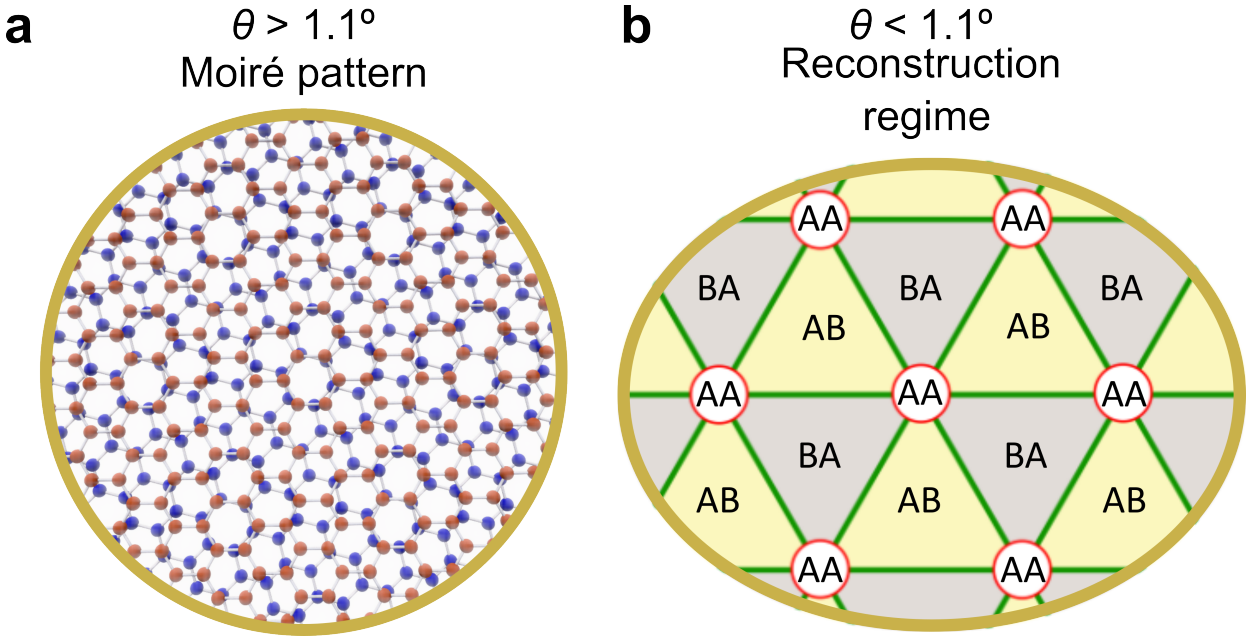

Fig. S 1: For θ greater than 1.1^{o}, the TBG structure reveals Moiré patterns. Below 1.1^{o}, the TBG unveils the reconstruction regime.

2 Nonlocal optical conductivity for twisted bilayer graphene

As stated in the main paper, the high degree of confinement factors implies that nonlocal effects can play an important role in the plasmon dispersion relation [4]. From the Kubo formula, a Drude-type frequency dependence for the intraband contribution to the optical conductivity of TBG was already been obtained [5]. Here, due to the talc substrate, the TBG sample will be doped [6] and we can expect, due to the Pauli blocking, for the vanishing of the interband component of the optical conductivity. A simple model that corresponds to the Drude conductivity in the limit of vanishing quantum corrections but takes in account nonlocal contributions is the hydrodynamical model [7]. Here, we will follow Ref. [8], where the hydrodynamic model was derived for monolayer graphene starting from the Boltzmann formalism, but now considering the TBG electrons. We start from the Drude mass defined as $m_D \equiv \hbar k_F/v_F$, with k_F being Fermi's momentum and v_F the Fermi velocity. The Drude mass correctly captures the light-matter coupling in this semiclassical approximation. The system is characterized by an electronic density n and velocity field $\mathbf{v}$. We consider an impinging monochromatic electron field $\mathbf{E}$ with frequency ω and wavevector $\mathbf{k}$.

Starting from Euler's equation for the graphene electrons [8]:

$$m_D n \frac{\partial \mathbf{v}}{\partial t} + m_D n \mathbf{v} \cdot \boldsymbol{\nabla} \mathbf{v} = \mathbf{g} m_D n - \boldsymbol{\nabla} P, \tag{1}$$

with $\mathbf{g}$ being the external forces and P the internal quantum pressure of the electron gas. Considering only the action of an external electric field, we have $\mathbf{g} = -e\mathbf{E}$.

In the linear regime the term quadratic in $\mathbf{v}$ does not contribute, and considering the presence of a scattering rate γ, we make $\partial_t \to \partial_t + \gamma$, thus:

$$m_D n \left(\frac{\partial}{\partial t} + \gamma \right) \mathbf{v} = -en\mathbf{E} - \boldsymbol{\nabla} P. \tag{2}$$

Considering that the pressure P depends only on the density n, we can expand P as:

$$P \approx P_0 + \left. \frac{\delta P}{\delta n} \right|_{n=n_0} \delta n, \tag{3}$$

with $\delta n \equiv n - n_0$, n_0 being the equilibrium density, and δn being the density fluctuation. Now we consider that the external electric field, the velocity field , and the density fluctuations have the dependence of $e^{i\mathbf{k}\cdot\mathbf{r}}$, with $\mathbf{r}$ being the TBG in-plane coordinates and $\mathbf{q}$ the in-plane wavenumber, i.e., we have:

$$\mathbf{E} = \mathbf{E}_1 e^{i\mathbf{k}\cdot\mathbf{r} - i\omega t}, \tag{4a}$$

$$n = n_0 + n_1 e^{i\mathbf{k}\cdot\mathbf{r} - i\omega t}, \tag{4b}$$

$$\mathbf{v} = \mathbf{v}_1 e^{i\mathbf{k}\cdot\mathbf{r} - i\omega t}, \tag{4c}$$

where $\mathbf{E}_1, n_0, n_1, \mathbf{v}_1$ are constants in the $\mathbf{r}, t$ variables. In this equation we considered only the in-plane component of the electric field.

Substituting Eq. (3) in (2) and retaining only the linear terms, we have:

$$-i m_D n_0 \left(\omega + \frac{1}{\tau} \right) \mathbf{v} = -e n_0 \mathbf{E}_1 - iB\mathbf{k}n, \tag{5}$$

where we defined $B \equiv \left. \frac{\delta P}{\delta n} \right|_{n=n_0}$.

The relation between n and $\mathbf{v}$ can be obtained from the continuity equation:

$$\boldsymbol{\nabla} \cdot (n\mathbf{v}) + \frac{\partial n}{\partial t} = 0, \tag{6}$$

which results in the linear response:

$$n_0 \mathbf{k} \cdot \mathbf{v}_1 - \omega n_1 = 0. \tag{7}$$

From Eqs. (5) and (7), we obtain the velocity field as:

$$\mathbf{v} = \frac{-en_0}{D} \begin{pmatrix} m_D n_0(-i\omega + \gamma) + iBk_y^2/\omega & -iBk_x k_y/\omega \\ -iBk_x k - y/\omega & m_D n_0(-i\omega + \gamma) + iBk_x^2/\omega \end{pmatrix} \mathbf{E_0}, \tag{8}$$

with

$$D = -m_D^2 n_0^2 \left(\omega + i\gamma\right)^2 + m_D n_0 (\omega + i\gamma) B k^2/\omega. \tag{9}$$

We now define $\beta^2 \equiv B/(mn_0)$, with β having dimension of speed. The linear current is given by $\mathbf{J} = -en_0\mathbf{v}$, which results in the nonlocal optical conductivity:

$$\sigma(\mathbf{k},\omega) = \frac{ie^2 n_0}{m_D(\omega+i\gamma)} \frac{1}{\omega(\omega+i\gamma) - \beta^2 k^2} \begin{pmatrix} (\omega+i\gamma)\omega - \beta^2 k_y^2 & \beta^2 k_x k_y \\ \beta^2 k_x k_y & (\omega+i\gamma)\omega - \beta^2 k_x^2 \end{pmatrix}. \tag{10}$$

The term βk that appears in the above expression corresponds to the diffusion of electrons due to the quantum pressure, and it is the origin of the nonlocal optical response. In the limit $\beta \to 0$, the optical conductivity (12) becomes the Drude conductivity:

$$\sigma_D(\omega) = \frac{ie^2 n_0}{m_D(\omega+i\gamma)} \begin{pmatrix} 1 & 0 \\ 0 & 1 \end{pmatrix}, \tag{11}$$

substituting the Drude mass $m_D = \hbar k_F/v_F$ and the electronic density $n_0 = 2k_F^2/\pi$, that takes into account spin, valley, and layer degrees of freedom, we obtain:

$$\sigma_D(\omega) = \frac{2\pi e^2}{\hbar(\omega+i\gamma)} \begin{pmatrix} 1 & 0 \\ 0 & 1 \end{pmatrix}, \tag{12}$$

that corresponds to twice the monolayer graphene intraband optical conductivity [9], as we are taking into account the two layers of TBG.

3 Transfer Matrix Method (TMM)

We consider a graphene layer deposited on a talc flake over a SiO_2 substrate. The dielectric function of the talc [10] is given by:

$$\epsilon_{\text{talc}}(\omega) = \begin{pmatrix} \epsilon_{\parallel}(\omega) & 0 & 0 \\ 0 & \epsilon_{\parallel}(\omega) & 0 \\ 0 & 0 & \epsilon_{\perp}(\omega) \end{pmatrix}, \tag{13}$$

with:

$$\epsilon_{\parallel}(\omega) = \epsilon_{\parallel,\infty} \left(1 + \frac{\omega_{\text{LO},\parallel}^2 - \omega_{\text{TO},\parallel}^2}{\omega_{\text{TO},\parallel}^2 - \omega^2 - i\omega\gamma_{\parallel}}\right), \tag{14}$$

$$\epsilon_{\perp}(\omega) = \epsilon_{\perp,\infty} \left(1 + \sum_{j=1}^{2} g_n \frac{\omega_{\text{LO},j}^2 - \omega_{\text{TO},j}^2}{\omega_{\text{TO},j}^2 - \omega^2 - i\omega\gamma_j}\right), \tag{15}$$

with $\varepsilon_{\parallel,\infty} = 2.5$, $\omega_{\mathrm{TO},\parallel} = 1011$ cm^{-1}, $\omega_{\mathrm{LO},\parallel} = 1041$ cm^{-1}, $\gamma_{\parallel} = 15$ cm^{-1} $\omega_{\mathrm{TO},1} = 948$ cm^{-1}, $\omega_{\mathrm{LO},1} = 1002$ cm^{-1}, $\omega_1 = 20$ cm^{-1}, $\omega_{\mathrm{TO},2} = 671$ cm^{-1}, $\omega_{\mathrm{LO},2} = 685$ cm^{-1}, $\omega_2 = 5$ cm^{-1}, $g_1 = 1$, $g_2 = 2.4$.

The SiO_2 infrared dielectric function is given by [11]:

$$\epsilon_{\mathrm{SiO_2}} = \epsilon_\infty \sum_{n=1}^{3} \frac{f_n \omega_{\mathrm{TO},n}^2}{\omega_{\mathrm{TO},n}^2 - \omega^2}, \tag{16}$$

with $\epsilon_\infty = 2.4$, $\omega_{\mathrm{TO}} = [448, 791.7, 1128.1]$ cm^{-1}, and $f_n = [0.7514, 0.1503, 0.6011]$.

We consider a transverse magnetic (TM) polarization, and that the heterostructure stacking is in the z direction and that the in-plane propagation direction is in the x direction. Considering that the H field is piecewise continuous along the z direction and point in the y direction, we have:

$$H_y = e^{iqx - i\omega t} \times \begin{cases} H_1^+ e^{ik_1 z} + H_1^- e^{-ik_1 z}, \text{ if } z < 0, \\ H_2^+ e^{ik_2 z} + H_2^- e^{-ik_2 z}, \text{ if } 0 < z < h, \\ H_3^+ e^{ik_3 (z-h)} + H_3^- e^{-ik_3 (z-h)}, \text{ if } z > h, \end{cases} \tag{17}$$

where h is the talc thickness and:

$$k_1 = \sqrt{k_0^2 - q^2}, \tag{18}$$

$$k_2 = \sqrt{\epsilon_\parallel k_0^2 - \frac{\epsilon_\parallel}{\epsilon_\perp} q^2}, \tag{19}$$

$$k_3 = \sqrt{\epsilon_{\mathrm{SiO_2}} k_0^2 - q^2}. \tag{20}$$

The electric displacement field can be obtained from $\boldsymbol{\nabla} \times \mathbf{H} = -i\omega \mathbf{D}$ and its x and z components are:

$$D_x = \frac{1}{\omega} e^{iqx - i\omega t} \times \begin{cases} k_1 H_1^+ e^{ik_1 z} - k_1 H_1^- e^{-ik_1 z}, \text{ if } z < 0, \\ k_2 H_2^+ e^{ik_2 z} - k_2 H_2^- e^{-ik_2 z}, \text{ if } 0 < z < h, \\ k_3 H_3^+ e^{ik_3 (z-h)} - k_3 H_3^- e^{-ik_3 (z-h)}, \text{ if } z > h, \end{cases} \tag{21}$$

$$D_z = -\frac{q}{\omega} e^{iqx - i\omega t} \times \begin{cases} H_1^+ e^{ik_1 z} + H_1^- e^{-ik_1 z}, \text{ if } z < 0, \\ H_2^+ e^{ik_2 z} + H_2^- e^{-ik_2 z}, \text{ if } 0 < z < h, \\ H_3^+ e^{ik_3 (z-h)} + H_3^- e^{-ik_3 (z-h)}, \text{ if } z > h, \end{cases} \tag{22}$$

Therefore, the electric field is given by:

$$E_x = \frac{1}{\epsilon_0 \omega} e^{iqx - i\omega t} \times \begin{cases} k_1 H_1^+ e^{ik_1 z} - k_1 H_1^- e^{-ik_1 z}, \text{ if } z < 0, \\ \frac{k_2}{\epsilon_\parallel} H_2^+ e^{ik_2 z} - \frac{k_2}{\epsilon_\parallel} H_2^- e^{-ik_2 z}, \text{ if } 0 < z < h, \\ \frac{k_3}{\epsilon_{\mathrm{SiO_2}}} H_3^+ e^{ik_3 (z-h)} - \frac{k_3}{\epsilon_{\mathrm{SiO_2}}} H_3^- e^{-ik_3 (z-h)}, \text{ if } z > h, \end{cases} \tag{23}$$

$$E_z = -\frac{q}{\epsilon_0\omega}e^{iqx-i\omega t} \times \begin{cases} H_1^+ e^{ik_1 z} + H_1^- e^{-ik_1 z}, \text{ if } z < 0, \\ \frac{1}{\epsilon_\perp} H_2^+ e^{ik_2 z} + \frac{1}{\epsilon_\perp} H_2^- e^{-ik_2 z}, \text{ if } 0 < z < h, \\ \frac{1}{\epsilon_{SiO_2}} H_3^+ e^{ik_3(z-h)} + H_3^- \frac{1}{\epsilon_{SiO_2}} e^{-ik_3(z-h)}, \text{ if } z > h. \end{cases} \tag{24}$$

From the boundary conditions we have for the air-graphene-talc interface [9]:

$$H_y|_{z=0^-} - H_y|_{z=0^+} = \sigma_{xx} E_x|_{z=0}, \tag{25}$$

and the continuity of the tangent electric field

$$E_x|_{z=0^-} - E_x|_{z=0^+} = 0, \tag{26}$$

which, after substituting Eqs. (17) and (23) in Eqs. (25) and (26), results in:

$$H_1^+ + H_1^- - H_2^+ - H_2^- = \sigma_{xx}\frac{k_1}{\varepsilon_0\omega}\left(H_1^+ - H_1^-\right), \tag{27}$$

$$k_1\left(H_1^+ - H_1^-\right) - \frac{k_2}{\epsilon_\parallel}\left(H_2^+ - H_2^-\right) = 0, \tag{28}$$

which results in:

$$H_2^+ = \frac{1}{2}\left(1 + \frac{k_1\varepsilon_\parallel}{k_2} - \sigma_{xx}\frac{k_1}{\varepsilon_0\omega}\right)H_1^+ + \frac{1}{2}\left(1 - \frac{\varepsilon_\parallel k_1}{k_2} + \sigma_{xx}\frac{k_1}{\varepsilon_0\omega}\right)H_1^-, \tag{29}$$

$$H_2^- = \frac{1}{2}\left(1 - \frac{\epsilon_\parallel k_1}{k_2} - \sigma_{xx}\frac{k_1}{\varepsilon_0\omega}\right)H_1^+ + \frac{1}{2}\left(1 + \frac{\epsilon_\parallel k_1}{k_2} + \sigma_{xx}\frac{k_1}{\varepsilon_0\omega}\right)H_1^-, \tag{30}$$

and we can put in the matrix formulation as:

$$\begin{pmatrix} H_2^+ \\ H_2^- \end{pmatrix} = \begin{pmatrix} \frac{1}{2}\left(1 + \frac{k_1\varepsilon_\parallel}{k_2} - \sigma_{xx}\frac{k_1}{\varepsilon_0\omega}\right) & \frac{1}{2}\left(1 - \frac{\varepsilon_\parallel k_1}{k_2} + \sigma_{xx}\frac{k_1}{\varepsilon_0\omega}\right) \\ \frac{1}{2}\left(1 - \frac{\epsilon_\parallel k_1}{k_2} - \sigma_{xx}\frac{k_1}{\varepsilon_0\omega}\right) & \frac{1}{2}\left(1 + \frac{\epsilon_\parallel k_1}{k_2} + \sigma_{xx}\frac{k_1}{\varepsilon_0\omega}\right) \end{pmatrix} \begin{pmatrix} H_1^+ \\ H_1^- \end{pmatrix}. \tag{31}$$

For the talc-SiO_2 interface, we have, from the boundary conditions:

$$H_y|_{z=h^-} - H_y|_{z=h^+} = 0, \tag{32a}$$

$$E_x|_{z=h^-} - E_x|_{z=h^+} = 0, \tag{32b}$$

which results in:

$$H_2^+ e^{ik_2 h} + H_2^- e^{-ik_2 h} - H_3^+ - H_3^- = 0, \tag{33}$$

$$\frac{k_2}{\epsilon_\parallel}\left(H_2^+ e^{ik_2 h} - H_2^- e^{-ik_2 h}\right) - \frac{k_3}{\epsilon_{SiO_2}}\left(H_3^+ - H_3^-\right) = 0, \tag{34}$$

which results in:

$$\begin{pmatrix} H_3^+ \\ H_3^- \end{pmatrix} = \begin{pmatrix} \left(1 + \frac{\epsilon_{SiO_2} k_2}{k_3 \epsilon_\parallel}\right) e^{ik_2 h} & \left(1 - \frac{\epsilon_{SiO_2} k_2}{k_3 \epsilon_\parallel}\right) e^{-ik_2 h} \\ \left(1 - \frac{\epsilon_{SiO_2} k_2}{k_3 \epsilon_\parallel}\right) e^{+ik_2 h} & \left(1 + \frac{\epsilon_{SiO_2} k_2}{k_3 \epsilon_\parallel}\right) e^{-ik_2 h} \end{pmatrix} \begin{pmatrix} H_2^+ \\ H_2^- \end{pmatrix}. \tag{35}$$

From the transfer matrix of Eqs. (31) and (35) we obtain the total transfer matrix $M = [m_{ij}]$, and using that the Fresnel reflection coefficient is given by $r_p = -m_{21}/m_{22}$, we can obtain the Loss function as $\mathcal{L} = -\text{Im}[r_p]$, whose results are presented in the next section.

4 Polaritonic spectra: Loss function

In Fig. S2, we show the polariton spectrum obtained from the Loss function as defined in the previous section for the graphene-talc-SiO_2 heterostructure. The blue dots are the experimental data. In Fig. S2a, we considered the hydrodynamic model for graphene with fitted β and E_F parameters, such as $\beta = 3.85 \times 10^6$ m/s and $E_F = 0.4$ eV. The obtained result reveals a good agreement with the experimental data further confirming that we can safely neglect interband contributions to the optical conductivity, as the Pauli blocking inhibits interband transitions with frequencies below $2E_F/\hbar =\approx 6400$ cm^{-1}. In Fig. S2b, we considered the Drude conductivity for graphene, i.e., making $\beta = 0$. In this case, the graphene plasmon branch appears in the 300-400 cm^{-1} range and does not hybridize with the talc phonons. In Fig. S2c, we also used the Drude model, but now fitting the Fermi energy, obtaining a very high value of $E_F = 4.0$ eV. In this case, the agreement is poorer, where the data above the phonon line at 948 cm^{-1} does not fit the plasmon dispersion.

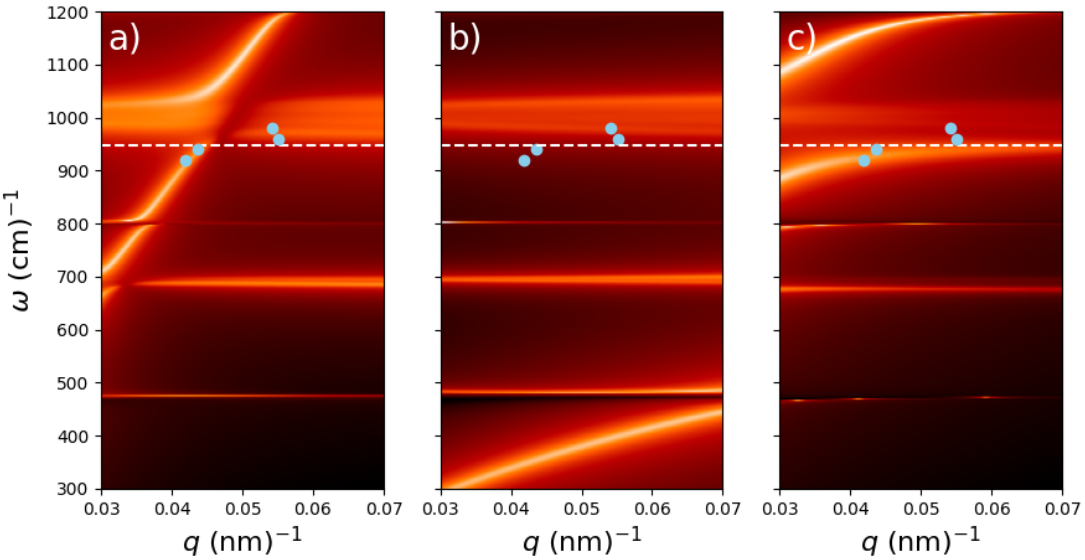

Fig. S 2: Loss function for the TBG-talc-SiO_2 heterostructure considering the TMM approach for different models of TBG conductivity. For each panel we considered the Fermi level at the graphene as a fitting parameter. The blue dots are the experimental data, as explained in the main paper. In panel a) we considered the hydrodynamic model for TBG graphene, and E_F and β as fitting parameters, which revealed the best agreement with our experimental data. In panel *b*) we used the same value of E_F of panel a), but for the Drude conductivity. In panel c) we show the best fit obtained using the Drude conductivity. The white dashed line marks the beginning of the first talc's Reststrahlen band [10].

We can conclude that the hydrodynamic model, which takes into account nonlocal contributions, can explain the experimental results, while it is impossible to obtain fits for the experimental data only considering the Drude conductivity of TBG. This work motivates further experimental and theoretical investigation of the microscopic description of the quantum pressure for TBG electrons.

References

[1] Yuan Cao, Valla Fatemi, Ahmet Demir, Shiang Fang, Spencer L. Tomarken, Jason Y. Luo, Javier D. Sanchez-Yamagishi, Kenji Watanabe, Takashi Taniguchi, Efthimios Kaxiras, Ray C. Ashoori, and Pablo Jarillo-Herrero. Correlated insulator behaviour at half-filling in magic-angle graphene superlattices. *Nature*, 556(7699):80–84, Apr 2018.

[2] Fernando Gargiulo and Oleg V Yazyev. Structural and electronic transformation in low-angle twisted bilayer graphene. *2D Materials*, 5(1):015019, nov 2017.

[3] Shuyang Dai, Yang Xiang, and David J. Srolovitz. Twisted bilayer graphene: Moiré with a twist. *Nano Letters*, 16(9):5923–5927, 2016. PMID: 27533089.

[4] Mark B. Lundeberg, Yuanda Gao, Reza Asgari, Cheng Tan, Ben Van Duppen, Marta Autore, Pablo Alonso-González, Achim Woessner, Kenji Watanabe, Takashi Taniguchi, Rainer Hillenbrand, James Hone, Marco Polini, and Frank H. L. Koppens. Tuning quantum nonlocal effects in graphene plasmonics. *Science*, 357(6347):187–191, 2017.

[5] Pietro Novelli, Iacopo Torre, Frank HL Koppens, Fabio Taddei, and Marco Polini. Optical and plasmonic properties of twisted bilayer graphene: Impact of interlayer tunneling asymmetry and ground-state charge inhomogeneity. *Physical Review B*, 102(12):125403, 2020.

[6] Edrian Mania, Ananias B Alencar, Alisson Ronieri Cadore, Bruno R. Carvalho, K. Watanabe, Takashi Taniguchi, Bernardo Ruegger Almeida Neves, Hélio Chacham, and Leonardo C. Campos. Spontaneous doping on high quality talc-graphene-hbn van der waals heterostructures. *2D Materials*, 4, 2017.

[7] N. Asger Mortensen. Mesoscopic electrodynamics at metal surfaces. *Nanophotonics*, 10(10):2563–2616, 2021.

[8] A. J. Chaves, N. M. R. Peres, G. Smirnov, and N. Asger Mortensen. Hydrodynamic model approach to the formation of plasmonic wakes in graphene. *Phys. Rev. B*, 96:195438, Nov 2017.

[9] Nuno MR Peres, P Andre D Gonçalves, Tobias Stauber, and N Asger Mortensen. Graphene plasmonics: manipulating light at the nanoscale with a one-atom-thick material. *Europhysics News*, 55(4):16–19, 2024.

[10] Flávio H. Feres, Francisco C. B. Maia, Shu Chen, Rafael A. Mayer, Maximillian Obst, Osama Hatem, Lukas Wehmeier, Tobias Nörenberg, Matheus S. Queiroz, Victor Mazzotti, J. Michael Klopf, Susanne C. Kehr, Lukas M. Eng, Alisson R. Cadore, Rainer Hillenbrand, Raul O. Freitas, and Ingrid D. Barcelos. Two-dimensional talc as a natural hyperbolic material, 2025. arXiv:2501.17340.

[11] Isaac John Luxmoore, Choon How Gan, Peter Qiang Liu, Federico Valmorra, Penglei Li, Jérôme Faist, and Geoffrey R. Nash. Strong coupling in the far-infrared between graphene plasmons and the surface optical phonons of silicon dioxide. *ACS Photonics*, 1(11):1151–1155, Nov 2014.